Nano Energy (2015) 13, 226–232

Available online at www.sciencedirect.com

ScienceDirect

journal homepage: www.elsevier.com/locate/nanoenergy

RAPID COMMUNICATION

High index of refraction nanosphere coatings for light trapping in crystalline silicon thin film solar cells

Baomin Wang, Paul W. Leu*

Department of Industrial Engineering, University of Pittsburgh, Pittsburgh, PA 15261, United States

Received 30 July 2014; received in revised form 19 August 2014; accepted 4 October 2014
Available online 24 February 2015

KEYWORDS
c-Silicon;
Photovoltaics;
Dielectric nanospheres;
Solar cells

Abstract
Dielectric nanospheres have emerged as a promising candidate for enhancing absorption in thin film photovoltaics. In this paper, we utilize numerical electrodynamic simulations to investigate the absorption enhancements achievable in crystalline Si (c-Si) thin films of thicknesses from 100 to 2000 nm from 2-dimensional close-packed silica (SiO_2), silicon nitride (Si_3N_4), and titania (TiO_2) nanosphere array coatings. We demonstrate that dielectric nanospheres can enhance the absorption in c-Si thin films by coupling incident light to transverse electric (TE) waveguide modes in the c-Si thin film. While SiO_2 nanosphere arrays may achieve enhancements of less than 10% compared to ideal double pass c-Si thin films, higher index of refraction nanospheres confine light more strongly such that more nanosphere resonances may couple to waveguide modes in the c-Si. Si_3N_4 nanospheres may enhance ultimate efficiencies by over 40% for thicknesses ≤ 800 nm and TiO_2 nanospheres by over 50% for thicknesses ≤ 700 nm compared to thin film structures with perfect anti-reflection coatings. This light trapping approach increases the absorption in the photoactive region without introducing additional surfaces or interfaces that increase surface recombination.

Introduction

One of the main challenges with the use of crystalline silicon (c-Si) for thin film photovoltaics is that c-Si is not a strong absorber of sunlight in the near-infrared region. Si is an indirect band gap material and thus photons with energy just above the band gap require phonon interactions for absorption. Si has absorption lengths $L_\alpha > 10$ μm for photons with wavelength $\lambda > 800$ nm and $L_\alpha > 100$ μm for $\lambda > 970$ nm. Different light trapping strategies are thus important for increasing the photon optical length, the distance a photon travels in the c-Si before escaping, in order to increase absorption. Light trapping helps reduce manufacturing costs

*Corresponding author.
E-mail address: pleu@pitt.edu.com (P.W. Leu).
URL: http://www.pitt.edu/~pleu/Research/ (P.W. Leu).

http://dx.doi.org/10.1016/j.nanoen.2014.10.040
2211-2855/

by improving efficiencies for a given active layer thickness. This allows for not only the use of less silicon, but more inexpensive silicon with shorter minority carrier diffusion lengths since carriers do not have to diffuse as far to be collected. Open circuit voltages are also expected to increase due to higher photocarrier injection levels. Manufacturing costs may be reduced while maintaining reasonable efficiencies.

Two of the main approaches to wave-optics light trapping in c-Si thin film solar cells has involved (1) structuring the active region and (2) using metal nanostructures. The first approach of structuring the photoactive region may be used to tune guided mode profiles to allow for greater field concentration inside the c-Si. New c-Si structures which use this approach have been demonstrated including nanowire arrays [1-9], nanocone arrays [10,11], nanohole arrays [12], and photonic crystals [13]. The second major approach involves the use of metal nanostructures for plasmonic light trapping through high near-fields, surface plasmon polaritons, and/or plasmonic scattering. Metal nanoparticles have been utilized to enhance optical absorption in single-crystalline silicon [14] and silicon-on-insulator [15] solar cells. Structures such as metal gratings [16,17], nanoparticle arrays [18], and nanogrooves [19] have also been shown to exhibit light trapping through simulations. However, both approaches to light trapping involve the use of additional manufacturing processes that may not be scalable. Metal nanostructures introduce additional reflection and parasitic absorption losses. More importantly, structuring the c-Si active region or introducing additional Si/metal interfaces results in higher internal losses due to increased surface recombination.

Recently, the Atwater group demonstrated a new approach to light trapping using sub-wavelength silica nanospheres coated on amorphous silicon (a-Si) [20] and gallium arsenide (GaAs) [21] thin films. These nanosphere arrays could offer benefits to cost reduction in thin film photovoltaics as they may be scalably coated onto the solar cell from a variety of nanosphere lithography approaches [22,23]. They may eliminate the need for an additional antireflection coating and enhance silicon absorption without introducing additional surface recombination.

However, in this study, the maximum enhancement was only about 15% for silica nanospheres on 100 nm thick a-Si compared with a-Si thin films with an antireflection coating layer and 11% for silica nanospheres on 100 nm thick GaAs compared to GaAs thin films with a double antireflection coating. Both a-Si and GaAs are direct band gap materials that are relatively strong absorbers of light even at thin thicknesses. In contrast, c-Si is an indirect band gap material, and solar cell thicknesses are typically several hundred microns to ensure absorption of most sunlight.

In this paper, we demonstrate significant efficiency enhancements in c-Si thin films with high index of refraction nanosphere arrays. The nanosphere arrays allow light to couple to transverse electric (TE) waveguide modes in the silicon. We perform simulations on close-packed silica (SiO_2), silicon nitride (Si_3N_4), and titania (TiO_2) nanosphere arrays to demonstrate that higher index of refraction nanospheres may achieve better light trapping. The higher index of refraction nanospheres exhibit stronger optical confinement and thus, more resonance modes may couple to TE waveguide modes in the c-Si. The periodicity and nanosphere resonances introduce wave vector components along the inplane directions, which allow light to couple to waveguide modes. We show that SiO_2 nanosphere arrays may achieve enhancements of less than 10% compared to an ideal double pass c-Si thin film. In contrast, higher index of refraction nanospheres such as Si_3N_4 may improve efficiency enhancements over 40% for c-Si thicknesses $t \leq 800$ nm and TiO_2 by over 50% for $t \leq 700$ nm. Si_3N_4 and TiO_2 nanospheres improve efficiencies by about 50% and over 100% respectively for c-Si thin films with $t = 100$ nm.

Results and discussion

Figure 1(a) shows a schematic of our simulated structure. A close packed monolayer of nanospheres with diameters d sits on top of a crystalline silicon (c-Si) thin film of thickness t. The nanosphere monolayer forms a hexagonal lattice. The lattice vectors are defined by $|a_1|=|a_2|=a$, and the angle between the two lattice vectors $\varphi = 60^\circ$. We assume the nanospheres are close-packed or d=a. We study a range of c-Si thicknesses t from 100 to 2000 nm (in increments of 100 nm) and nanosphere diameters d from 200 to 2000 nm (in increments of 20 nm). The

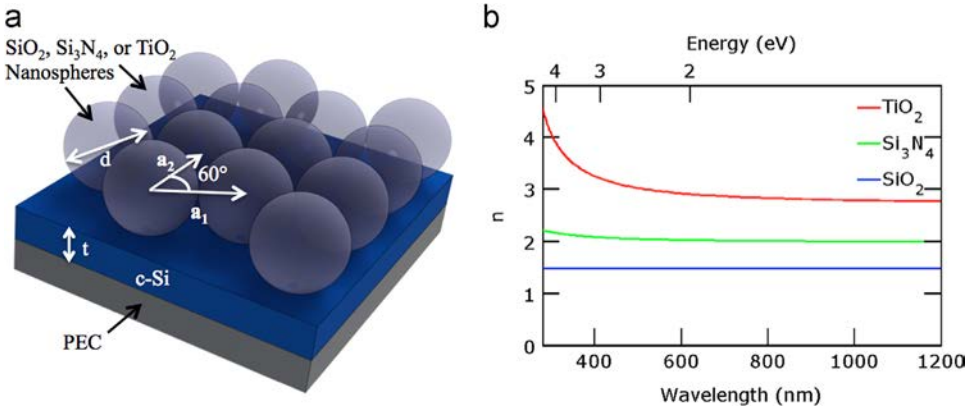

Figure 1 (a) Schematic of the dielectric nanosphere solar cell. The crystalline silicon (c-Si) thin film has thickness t and sits on top of a perfectly electrical conductor (PEC). A hexagonal close packed-monolayer of nanospheres lies on top of this thin film. The diameter of the nanospheres equals the pitch $d=a$. (b) Real part of the index of refraction n for the three nanospheres studied.

c-Si sits on top of a perfectly electric conductor (PEC). We studied SiO_2, Si_3N_4, and TiO_2 nanospheres and the real part of the index of refraction n is shown in Figure 1(b). The optical constants for c-Si, SiO_2, and Si_3N_4 are taken from data in Palik's *Handbook of Optical Constants of Solids* [24]. The optical constants for TiO_2 were also taken from the same source, though the optical constants are extrapolated out to 280 nm. SiO_2, Si_3N_4, and TiO_2 have indices of refraction of approximately 1.4, 2, and 3 respectively. The SiO_2 and Si_3N_4 are amorphous, while the TiO_2 is the rutile crystal structure. The imaginary part of the index of refraction for these three materials is 0, so that the nanospheres do not absorb any light. While TiO_2 does exhibit some absorption below 440 nm, the imaginary part of the index of refraction of TiO_2 was assumed to be 0 to simplify the analysis and focus the study on the effect of index of refraction change.

Appropriate symmetric and anti-symmetric boundary conditions were used to ensure the periodicity of the unit cell. From the simulations, we obtained the energy dependent reflection $R(E)$ and the absorption spectra was calculated from $A(E)=1-R(E)$. In order to evaluate the absorption performance of silicon solar cells across the solar spectrum, we calculated the ultimate efficiency from

$$\eta = \frac{\int_{E_g}^{\infty} I(E)A(E)((E_g/E)dE)}{\int_0^{\infty} I(E)dE} \quad (1)$$

where $E_g=1.12$ eV is the band gap of c-Si and $I(E)$ is the solar irradiance under the global 37° tilt Air Mass 1.5 spectrum [25]. We investigated the optical properties over the wavelength range from 280 to 1200 nm.

To begin with, we focused on simulating $t=200$ nm thick c-Si thin films and SiO_2 nanosphere arrays. In these simulations, we used a uniform grid size of $5\times5\times5$ nm^3. Figure 2(a) illustrates the absorption spectra for a 200 nm thick c-Si film. Resonant absorption peaks are found in the c-Si thin film on metal when the following condition is satisfied:

$$\tan(nkt) = -ni \quad (2)$$

where k is the free space wave number and n is the silicon index of refraction. The leaky modes of planar films are TEM modes labeled with mode number m as TEM_m. Interference leads to a resonant Fabry-Perot cavity effect within the film. These resonant modes are characterized by $m/2+1/4$ wavelengths in the transverse direction of the planar film, where the electric field intensity is at a maximum at the front surface and 0 at the back metal interface. The thin film absorption resonances for $m=1$ to 4 are shown and marked with the white dotted lines.

Then, we introduced SiO_2 nanospheres on top of this c-Si thin film. Figure 2(b) plots the absorption contour for the close-packed SiO_2 nanospheres as a function of diameter on top of the 200 nm thick c-Si film. Several additional absorption peaks that increase in wavelength with increasing nanosphere diameter can be seen. The best efficiency enhancement for the silica nanospheres on top of 200 nm thick c-Si is with $d=a=900$ nm, which is indicated with the black dashed line in Figure 2(b). Figure 2(c) plots the absorption spectra for these optimized SiO_2 nanospheres in blue. The green curve shows the absorption spectra for the 200 thick c-Si film without the nanospheres. The best efficiency enhancement occurs where there are many resonances just above the Si band gap, $E_g=1.12$ eV (or wavelengths slightly below $\lambda_g=1110$ nm).

The nanosphere coatings result in several additional resonance peaks in the absorption spectra. These resonance peaks are marked in Figure 2(c) with vertical light gray dotted lines. In order to understand the absorption enhancement at these thin films, we performed additional electric field intensity simulations. Figure 3 plots the real part of the electric field in the x-direction at the wavelengths associated with these modes. The incident light is polarized with electric field in the x-direction, and the real part of the electric field in the x-direction is plotted at λ=(a) 814, (b) 868, (c) 902, (d) 975, (e) 1008, and (f) 1067 nm. The top row plots a cross-section in the x-z plane through the center of a nanosphere ($y=0$ nm). The edges of the nanosphere and c-Si thin film are shown with black dashed lines. The bottom row plots a cross-section in the x-y plane through the center of the silicon ($z=100$ nm). The edges of the close-packed nanosphere array are shown with black dashed lines as well in these plots. The introduction of

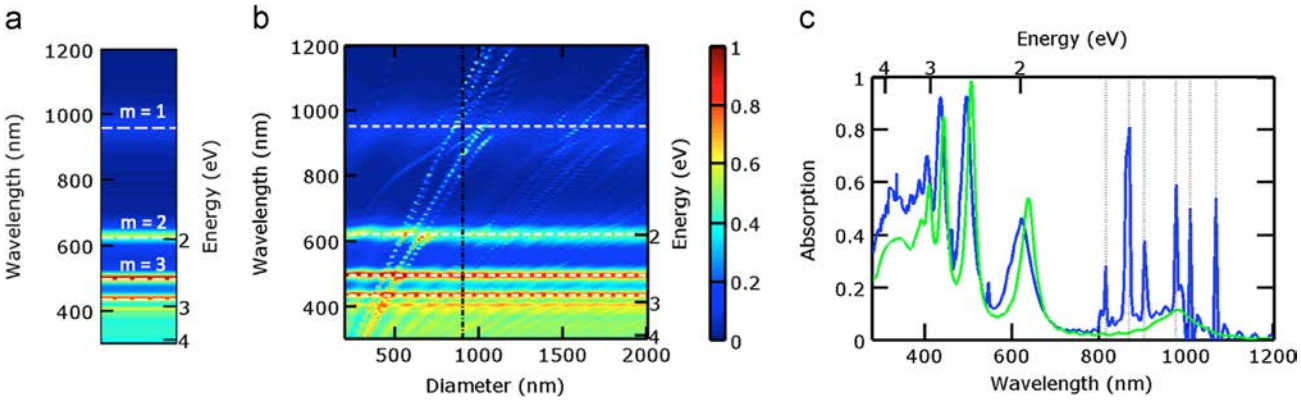

Figure 2 Absorption of (a) 200 nm thick c-Si and (b) 200 nm thick c-Si with different diameter close-packed SiO_2 nanosphere arrays on top. Thin film TEM_m modes are marked with white dashed lines. The optimal ultimate efficiency occurs for $d=a=900$ nm, marked with the black dash-dotted line. (c) Absorption spectra of the optimal SiO_2 nanosphere array in blue compared with the absorption spectra of 200 nm thick bare c-Si in green.

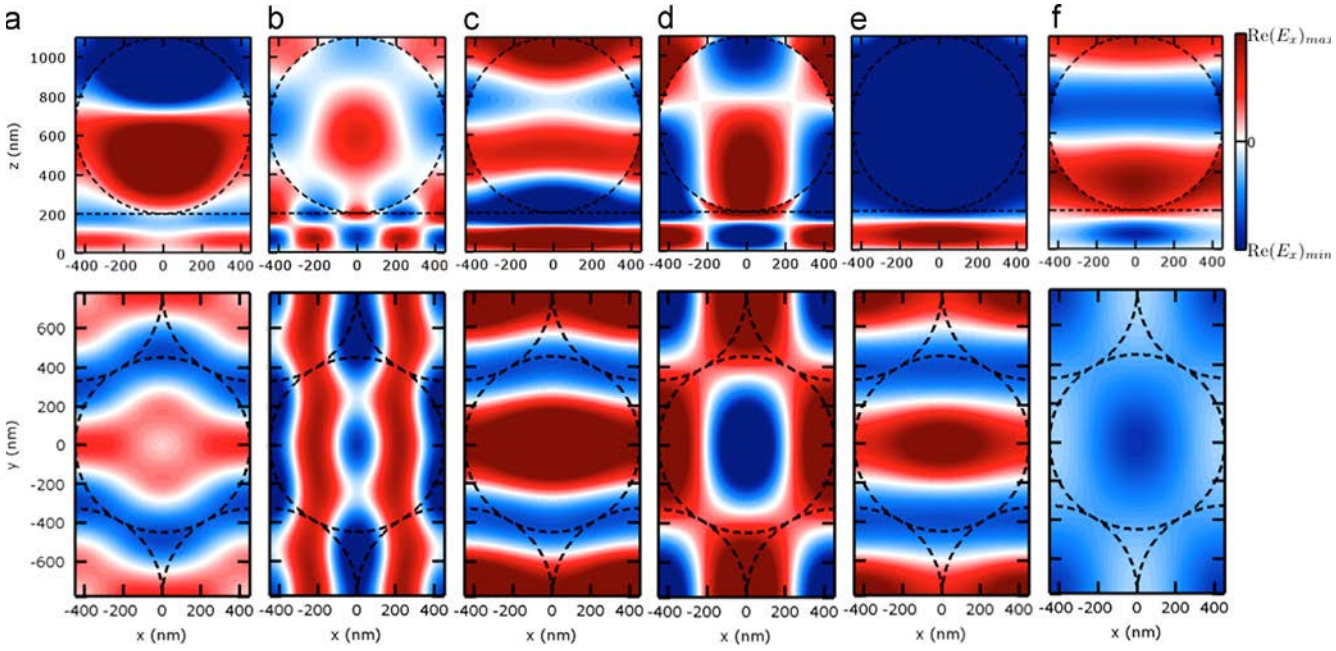

Figure 3 Real part of E_x for λ=(a) 814, (b) 868, (c) 902, (d) 975, (e) 1008, and (f) 1067 nm. The top row plots a cross-section in the x-z plane through the center of a nanosphere (y=0 nm). The bottom row plots a cross-section in the x-y plane through the center of the silicon (z=100 nm). The edges of the close-packed nanosphere array and c-Si thin film are shown with black dashed lines. The modes shown are TE_1 waveguide modes.

nanosphere arrays on the front of the c-Si thin film allows for the excitation of TE waveguide modes. In particular, the waveguide modes shown here are TE_1 waveguide modes, which are characterized by 3/4 wavelengths along the thickness of the c-Si, and E_x is a minimum at the back metal surface. Higher order TE_m waveguide modes are also excited at λ=545 and 460 nm for m=2 and 3 respectively, as can be seen in Figure 2(c) though these peaks are relatively small. Dielectric nanospheres may excite TE_m waveguide modes only, in contrast with metallic nanostructures, which can excite both TE_m and TM_m waveguide modes [17,18]. When the reciprocal lattice vector of the nanosphere array or the k-vector of the nanosphere resonances matches the k-vector of the c-Si waveguide mode, incoming radiation may be coupled into these waveguide modes, which enables light trapping.

Higher index of refraction nanospheres more strongly confine light so that there are more whispering gallery modes for a particular nanosphere diameter. Thus, we next investigate the absorption enhancement with silicon nitride (Si_3N_4) and titanium oxide (TiO_2) nanospheres. Figure 4(b) and (c) plots the absorption contour for close-packed Si_3N_4 and TiO_2 nanospheres respectively as a function of pitch on top of the 200 nm thick c-Si film. A larger number of optical dispersion lines corresponding to a larger number of modes appear for Si_3N_4 and TiO_2. The best efficiency enhancement for the Si_3N_4 nanospheres on top of 200 nm c-Si film is with d=a=720 nm. The absorption spectrum for this structure is shown in Figure 4(c) in blue, where the green curve again shows the absorption spectrum for the 200 nm c-Si film. The best efficiency enhancement for the TiO_2 nanospheres is with d=a=1040 nm. The absorption spectrum for this structure is shown in Figure 4(d) in blue, where the green curve again shows the absorption spectrum for the 200 nm c-Si film. The overall absorption is enhanced with the Si_3N_4 and even more with the TiO_2 nanospheres due to larger number of modes present. Table 1 shows the ultimate efficiency η, short circuit current J_{sc}, and solar absorption A_{solar} of the 200 nm c-Si thin film on back metal, ideal double pass c-Si, and 200 nm c-Si with optimized SiO_2, Si_3N_4, and TiO_2 nanospheres. The short circuit current is calculated from $J_{sc} = q\int_{E_g}^{\infty} b_s(E)A(E)dE$ and the solar absorption from $A_{solar} = \int_{E_g}^{\infty}(E)A(E)dE$ where b_s (E) is the photon flux density of the global Air Mass 1.5 spectrum [25]. The absorption of the ideal double pass thin film is

$$A(E) = 1 - \exp[2\alpha(E)t] \tag{3}$$

where $\alpha(E)$ is the energy dependent absorption coefficient of c-Si. The ideal double pass thin film assumes perfect antireflection at the front surface, $R(E)$=0, and perfect reflection at the back surface, $R(E)$=1. All nanosphere coatings exhibit light trapping properties with better absorption and ultimate efficiency than the ideal double pass and thin film Si. We also show in Table 1 the efficiency enhancements G_1 and G_2 of the various structures to thin film c-Si and ideal double pass c-Si respectively. Efficiency enhancements of over 50% or more are possible with Si_3N_4 and TiO_2 nanospheres compared to the ideal double pass c-Si thin film.

Finally, we evaluated the efficiency enhancements possible with nanosphere coatings over a range of c-Si thicknesses from t=100–2000 nm. These simulations were performed with a uniform grid size of $20 \times 20 \times 20\ \mathrm{nm}^3$, due to the large number of simulations that were performed. The ultimate efficiency was found to have converged within 2% with this grid size. Figure 5(a), (b), and (c) utilizes contour plots to illustrate the dependence of ultimate efficiency on the thickness of the c-Si and nanosphere diameter (which

is equal to the pitch) of the SiO_2, Si_3N_4, and TiO_2 nanosphere arrays respectively. The optimal ultimate efficiencies for each thickness of c-Si are marked with black circles in the contour plots. Figure 5(d) plots the optimum diameter for each c-Si thickness for the three different types of nanospheres. The best diameter for the SiO_2 nanospheres is about 900 nm and TiO_2 nanospheres is about 800 nm across the different thicknesses evaluated, while for Si_3N_4, the best diameter tends to increase with increasing c-Si thickness. In addition, based on the contour plots, we note that the efficiency is not that sensitive to the nanosphere diameter so long as the nanospheres are larger than some minimum diameter (about 700 nm). In Figure 5(e), we plot the best ultimate efficiencies of the c-Si thin film, ideal double pass c-Si, and the best nanosphere coatings as a function of c-Si thickness. The short-circuit current is plot on the right y-axis. The optimal ultimate efficiency enhancement G_2 of the different types of nanosphere coatings compared to the ideal double pass c-Si thin film are plot in Figure 5(f) for different c-Si film thicknesses. While the efficiency enhancement for SiO_2 is under 10% for all c-Si thicknesses, Si_3N_4 nanospheres may improve efficiencies by over 40% for c-Si thicknesses $t \leq 800$ nm and TiO_2 nanospheres by over 50% for $t \leq 700$ nm. The efficiency improvements decrease for larger c-Si thicknesses and are 1%, 23%, and 24% for SiO_2, Si_3N_4, and TiO_2 respectively for $t=2000$ nm. These simulations suggest that high index of refraction nanospheres may exhibit better light trapping properties than metal nanostructures, which have demonstrated enhancements of 43% in 50 nm [17] and 22% in 100 nm [18] thick c-Si. While metal nanostructures may enhance absorption by coupling incoming light into both TE_m and TM_m waveguide modes as well as the excitation of localized surface plasmon resonances, they also exhibit parasitic absorption and enhanced reflection.

Table 1 Comparison of the performance of 200 nm c-Si film on metal under different photon management schemes. η (%), J_{sc} (mA/cm^2), A_{solar} (%), and G_1, G_2.

Structure	η	J_{sc}	A_{solar}	G_1	G_2
Thin film	8.0	7.2	10.4	1.00	0.80
Ideal double pass	10.0	9.0	13.0	1.25	1.00
With SiO_2 nanospheres	11.1	9.9	14.2	1.38	1.10
With Si_3N_4 nanospheres	15.1	13.5	19.4	1.88	1.50
With TiO_2 nanospheres	17.5	15.6	22.1	2.18	1.74

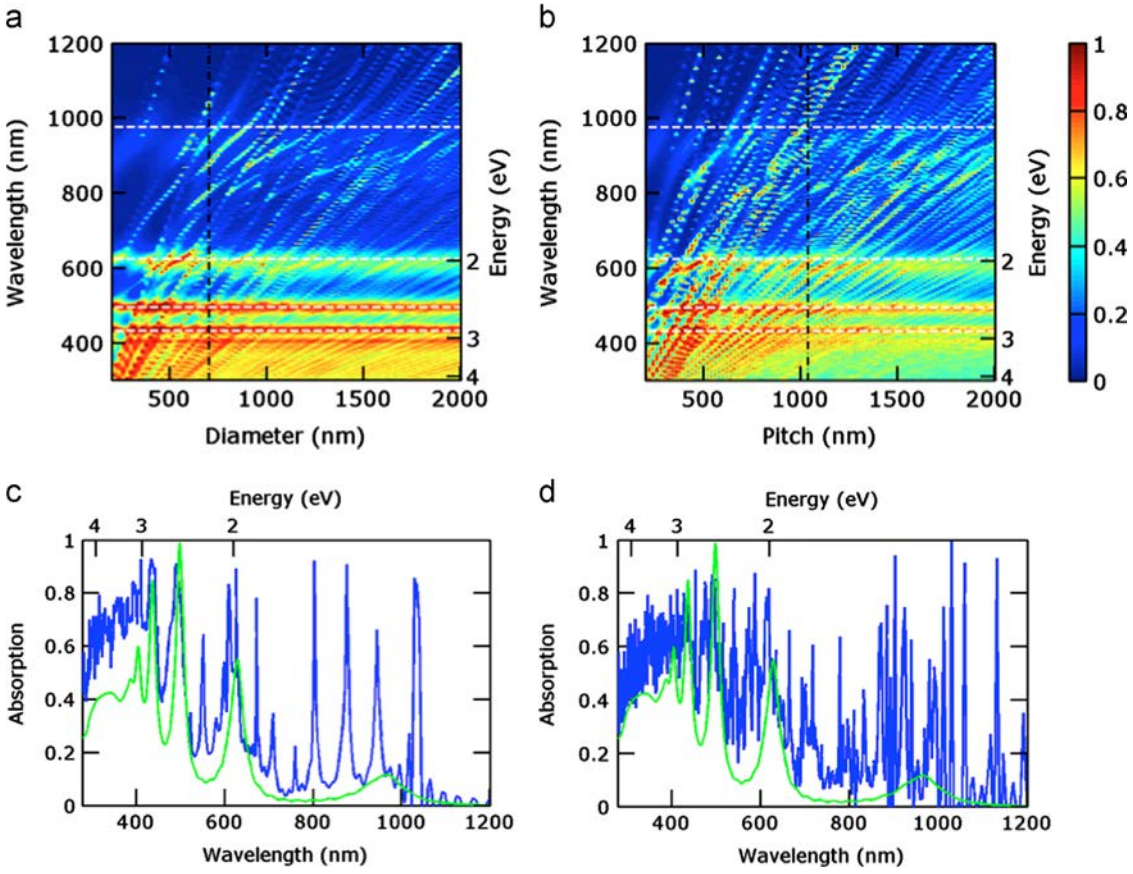

Figure 4 Absorption of 200 nm thick c-Si with different diameter close-packed (a) Si_3N_4 and (b) TiO_2 nanosphere arrays on top. The optimal ultimate efficiency occurs for $d=a=700$ nm and for $d=a=1040$ nm for the Si_3N_4 and TiO_2 nanospheres respectively, which are marked with the black dash-dotted lines. Absorption spectra of the optimal (c) Si_3N_4 and (d) TiO_2 nanosphere arrays in blue compared with the absorption spectra of 200 nm thick bare c-Si.

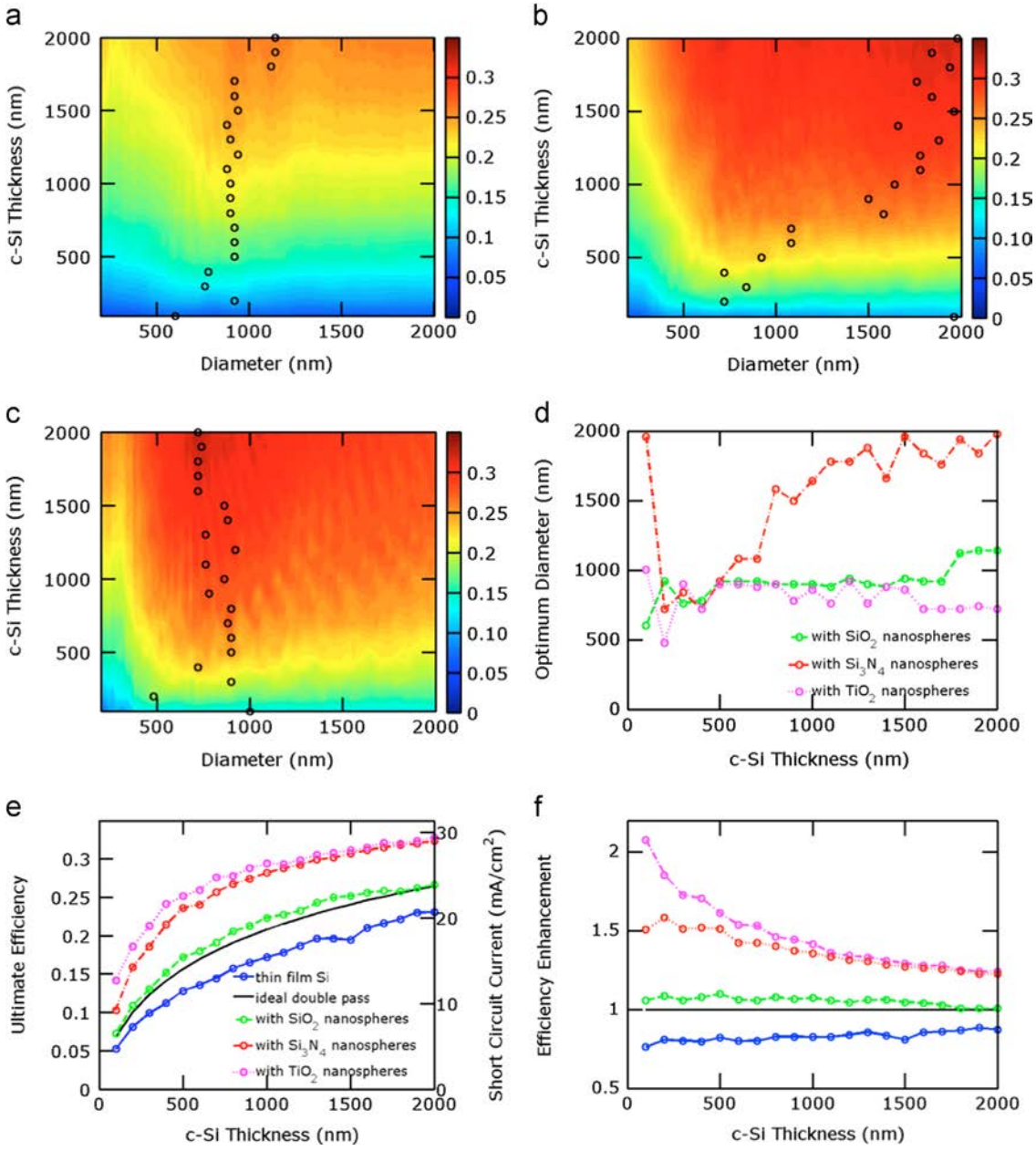

Figure 5 Ultimate efficiency η of c-Si thin film with (a) SiO_2, (b) Si_3N_4, and (c) TiO_2 close-packed nanospheres as a function of the c-Si thickness t and diameter d (which equals to the pitch a). The maximum efficiency of the solar cells for each thickness is shown with black circles. (d) Optimum diameter for different thicknesses of c-Si. (e) The maximum ultimate efficiency of various thickness c-Si solar cells as compared to an ideal double pass c-Si thin film and thin film c-Si on top of a perfect reflector. The short circuit current is shown on the right y-axis. (f) The ultimate efficiency enhancement G_2 from nanosphere coatings as compared to the ideal double pass thin film.

Conclusions

We investigated 2-dimensional periodic closed-packed SiO_2, Si_3N_4, and TiO_2 nanosphere arrays on c-Si thin films for enhancing the absorption in the c-Si photoactive region. By evaluating the electric field of absorption peaks in the nanosphere coated systems, we demonstrate that enhanced light trapping is due to the coupling of incident light to TE_m waveguide modes. We demonstrate that higher index of refraction nanospheres may achieve better light trapping since they have more resonant modes due to stronger optical confinement. Enhancements over 100% can be obtained on 100 nm thick c-Si films with TiO_2 nanospheres, though the enhancements decrease with thicker cells. This light trapping mechanism improves efficiencies without introducing new surfaces or interfaces that increase surface recombination as exhibited by other nanophotonic or plasmonic light trapping strategies.

Acknowledgment

This work was supported by the NSF award CMMI 1233151.

References

[1] V. Sivakov, G. Andrä, A. Gawlik, A. Berger, J. Plentz, F. Falk, S.H. Christiansen, Nano Lett. 9 (2009) 1549–1554.
[2] L. Tsakalakos, J. Balch, J. Fronheiser, B.A. Korevaar, O. Sulima, J. Rand, Appl. Phys. Lett. 91 (2007) 233117.
[3] T.H. Stelzner, M. Pietsch, G. Andra, F. Falk, E. Ose, S. Christiansen, Nanotechnology 19 (2008) 295203.
[4] K. Peng, Y. Xu, Y. Wu, Y. Yan, S. Lee, J. Zhu, Small 1 (2005) 1062–1067.
[5] E.C. Garnett, P. Yang, J. Am. Chem. Soc. 130 (2008) 9224–9225.
[6] E. Garnett, P. Yang, Nano Lett. 10 (2010) 1082–1087.
[7] O. Gunawan, S. Guha, Sol. Energy Mater. Sol. Cells 93 (2009) 1388–1393.
[8] M.D. Kelzenberg, S.W. Boettcher, J.A. Petykiewicz, D.B. Turner-Evans, M.C. Putnam, E.L. Warren, J.M. Spurgeon, R.M. Briggs, N.S. Lewis, H.A. Atwater, Nat. Mater. 9 (2010) 239–244.
[9] K.E. Plass, M.A. Filler, J.M. Spurgeon, B.M. Kayes, S. Maldonado, B.S. Brunschwig, H.A. Atwater, N.S. Lewis, Adv. Mater. 21 (2009) 325–328.
[10] B. Wang, P.W. Leu, Nanotechnology 23 (2012) 194003.
[11] C. Hsu, S.T. Connor, M.X. Tang, Y. Cui, Appl. Phys. Lett. 93 (2008) 133109.
[12] K. Peng, X. Wang, L. Li, X. Wu, S. Lee, J. Am. Chem. Soc. 132 (2010) 6872–6873.
[13] O. El Daif, E. Drouard, G. Gomard, A. Kaminski, A. Fave, M. Lemiti, S. Ahn, S. Kim, P. Roca i Cabarrocas, H. Jeon, C. Seassal, Opt. Express 18 (2010) A293–A299.
[14] D.M. Schaadt, B. Feng, E.T. Yu, Appl. Phys. Lett. 86 (2005) 063106.
[15] S. Pillai, K.R. Catchpole, T. Trupke, M.A. Green, J. Appl. Phys. 101 (2007) 093105.
[16] W. Wang, S. Wu, K. Reinhardt, Y. Lu, S. Chen, Nano Lett. 10 (2010) 2012–2018.
[17] R.A. Pala, J. White, E. Barnard, J. Liu, M.L. Brongersma, Adv. Mater. 21 (2009) 3504–3509.
[18] T. Gao, E. Stevens, J. kun Lee, P.W. Leu, Opt. Lett. 39 (2014) 4647–4650.
[19] V.E. Ferry, L.A. Sweatlock, D. Pacifici, H.A. Atwater, Nano Lett. 8 (2008) 4391–4397.
[20] J. Grandidier, D.M. Callahan, J.N. Munday, H.A. Atwater, Adv. Mater. 23 (2011) 1272–1276.
[21] J. Grandidier, D. Callahan, J. Munday, H.A. Atwater, IEEE J. Photovolt. 2 (2012) 123–128.
[22] J.C. Hulteen, J. Vac. Sci. Technol. A 13 (1995) 1553.
[23] C.L. Haynes, R.P. Van Duyne, J. Phys. Chem. B 105 (2001) 5599–5611.
[24] E.D. Palik, Handbook of Optical Constants of Solids, Academic Press, Orlando, 1997.
[25] Solar Spectral Irradiance: Air mass 1.5, URL: ⟨http://rredc.nrel.gov/solar/spectra/am1.5/⟩.

Baomin Wang received his Bachelor of Eng. from the department of Materials Science and Engineering, Tsinghua University, China, in 2010. He is currently pursuing his Ph.D. degree under Dr. Leu at the University of Pittsburgh, USA. His research focuses on simulation and experimental fabrication of nanostructured silicon solar cells.

Dr. Paul W. Leu received his B.S. in Mechanical Engineering from Rice University in 2002. He received his M.S. and Ph.D. from Stanford University in 2006 and 2008 respectively. From 2008–10, he worked as a postdoctoral fellow in the department of Electrical Engineering and Computer Sciences at the University of California, Berkeley with a joint appointment at Lawrence Berkeley National Laboratory. He has been an Assistant Professor in the Department of Industrial Engineering at the University of Pittsburgh since August, 2010. His research group's areas of expertise include solar cells, nanomanufacturing, and simulation-based design.